Effect of ultrasound on reverse leakage current of silicon Schottky barrier structure

O. Ya Olikh[1, †], K. V. Voitenko[1], R. M. Burbelo[1], and Ja M. Olikh[2]

[1]Faculty of Physics, Taras Shevchenko National University of Kyiv, Kyiv 01601, Ukraine
[2]V Lashkaryov Institute of Semiconductor Physics, National Academy of Sciences of Ukraine, Kyiv 03028, Ukraine

Abstract: The influence of ultrasonic loading on reverse current–voltage characteristics of Mo/n–n$^+$–Si structures has been investigated. The research of leakage current variation has been carried out for various ultrasonic wave frequencies (4.1 and 8.4 MHz), intensities (up to 0.8 W/cm^2) and loading temperatures (130–330 K). The observed reversible acoustically induced increase in reverse currents was as large as 60%. It has been found that dominant charge transfer mechanisms are the thermionic emission (at high temperature) and the phonon-assisted tunneling (at low temperature). The ultrasound loading affects both processes due to the decrease of Schottky barrier height and binding energy of the electron on the trap.

Key words: Schottky contact; leakage current; ultrasound influence
DOI: 10.1088/1674-4926/37/12/122002 **PACS:** 73.30.+y; 43.35.Ty; 43.35.+d **EEACC:** 2560

1. Introduction

Operating characteristics of semiconductor devices are known to be defined by the defect system mainly. The irradiation and annealing are most widespread and studied methods of alteration of semiconductor defects. In recent years, it has been shown experimentally that ultrasonic (US) waves affect various properties of semiconductors too. In particular, ultrasound is used to originate a negative differential resistance of bulk crystal[1], to modify a radiative process in quantum wells[2, 3], to correlate an electron transport in heterostructures[4, 5], to affect a carrier diffusion length[6, 7], to vary a tunneling[8, 9], a generation–recombination[10–12] and a thermionic emission (TE)[13, 14] current in p–n structures and Schottky diodes (SDs), to change a surface states spectrum[15] and density[16] of silicon-based structures, to transform a native[17, 18] and an impurity defect[19, 20]. Ultrasound as the effective tool has some advantages[13, 16]: (i) local effect due to the predominant ultrasound absorption in regions of deviation in the lattice periodicity; (ii) selectivity of the influence, which is achieved by variation of US wave polarization and type; (iii) possibility of resonance transformations in the defect system due to the oscillation nature of the process action.

Thus ultrasound can be the effective instrument for defect engineering. On the other hand, the leakage current is an important parameter of various semiconductor devices and has received much attention[21–25]. The majority of leakage current mechanisms in metal–semiconductor (MS) structures deal with a detects, located at the near interface region. They are the thermionic trap-assisted tunneling[21], the space-charge limited current (SCLC)[26, 27], the thermally-assisted variable-range-hopping conduction (VRHC)[22, 27, 28], and the phonon-assisted tunneling (PAT)[23, 29]. In addition, the TE current considerably depends on interfacial surface inhomogeneities too[30]. The goal of this study is experimental investigation of the reverse current in silicon SD under conditions of US loading (USL). The used US intensity was not very high to avoid the irreversible modification of SD properties. Both the acoustically induced (AI) reversible variation of the semiconductor structure characteristic and the wide temperature range of USL mark out this study against other works, which are devoted to the active ultrasound too. We believe that the idea of acoustic driving on the diode current could have particular electronic application and seem worth extending.

2. Experimental details

The samples used in our experiments were 0.2 μm thick n–Si:P epitaxial layer on 250 μm thick n$^+$–Si:Sb substrate. The substrate N_s and epi-layer N_d carrier concentration were 4.2×10^{22} and 7.25×10^{21} m^{-3} respectively. The square of molybdenum Schottky contact fabricated on the epi-layer surface was 7×7 mm^2.

The reverse current–voltage (I–V) characteristics of the samples both with and without US loading were measured in the temperature range from 130 to 330 K. In the case of US loading, the longitudinal waves excited in the samples were 4.1 and 8.4 MHz in frequency f_{US} and had the intensity of $W_{US} < 0.8$ W/cm^2. It was reported previously[3, 9, 14, 20] that a characteristic time of change in the silicon structure parameters under the ultrasound action did not exceed 2×10^3 s. In order to wait till the acoustically induced transitional period the following experimental procedure was used. After a USL start, the sample was kept at room temperature for 30 min. Then the sample was cooled to 130 K. The cooling time was about half an hour. After cooling, the I–V measurements and the sample heating were started. The sample temperature was controlled by differential copper-constantan thermocouple.

In order to avoid the effect of a piezoelectric field on I–V characteristics, the piezoelectric cell was shielded and an aluminum acoustic line was used. More details about the experimental setup are presented elsewhere[31].

The data non-linear fitting was done by using the differential evolution method[32].

† Corresponding author. Email: olikh@univ.kiev.ua
Received 12 February 2016, revised manuscript received 23 June 2016

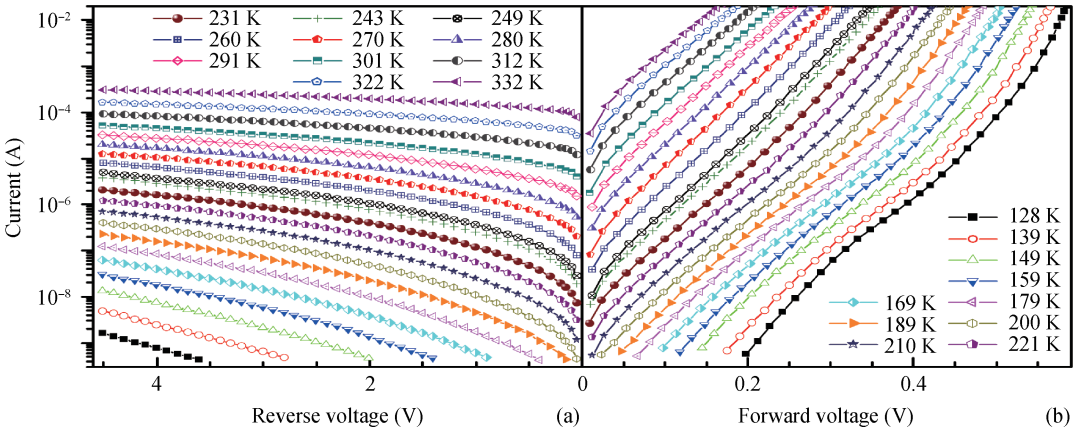

Figure 1. (Color online) (a) Reverse and (b) forward I–V characteristics of Mo/n–Si Schottky structures measured at 10 K intervals without USL. The lines are added to guide the eye.

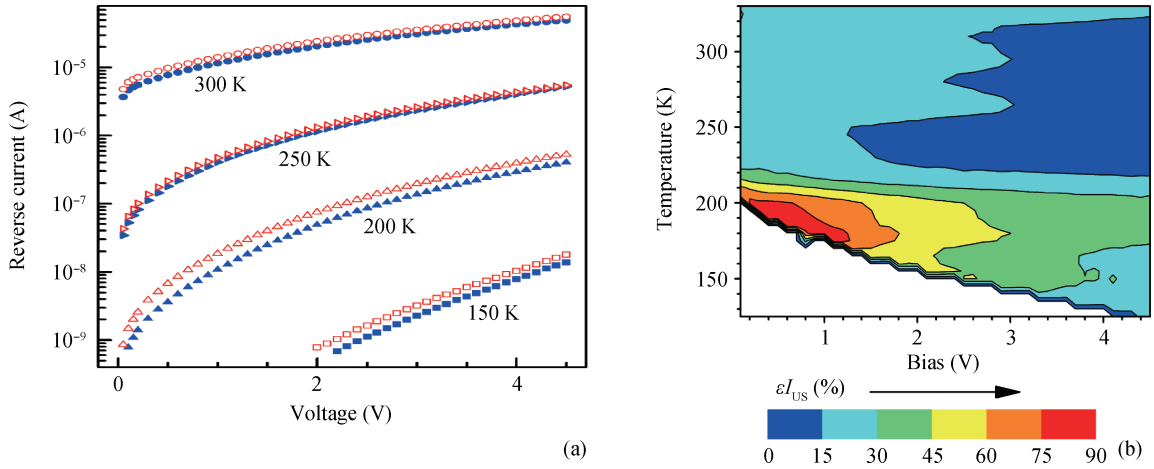

Figure 2. (Color online) (a) Reverse I–V characteristics measured with (open marks) and without (full marks) USL as a function of temperature. (b) Change of the relative AI current variation with the bias and the temperature. $f_{US} = 4.1$ MHz, $W_{US} = 0.65$ W/cm^2.

3. Results and discussion

3.1. Ultrasound influence on reverse current

Figure 1 shows the complete I–V–T characteristics that were measured without US loading. To avoid a busy-looking graph, the selection of measured I–V characteristics is shown in this figure. Below the reverse branches only are under consideration. It is a universal observation that the current from any SD never truly saturates at large reverse bias. Such "soft" reverse characteristics are observed for structures under investigation too. One can see that the reverse current change with the bias increase is larger at the low temperature.

As seen from Figure 2(a), US loading leads to the reverse current increase. The selection of I–V characteristics is shown in this figure. Ultrasound has been found to result in the reversible current variation, i.e., the current value has relaxed after US loading to the initial magnitude.

The ultrasound influence is described by the relative AI variation in the reverse current $\varepsilon I_{US} = (I_{R,US} - I_{R,0})/I_{R,0}$, where $I_{R,US}$ and $I_{R,0}$ are the reverse current at the same temperature with and without USL respectively.

Figure 2(b) shows the εI_{US} dependencies on the bias and the temperature. They are representative data for both used f_{US} values. It has been found that (i) the AI increase in the reverse current can reach several tens of percent; (ii) in the low temperature range the US influence efficiency falls off with bias as well as temperature increase; (iii) if the temperature is greater than 250 K then both temperature and bias dependence of εI_{US} is weak.

Figure 3 shows the εI_{US} change with the US intensity. We want to stress two features. Firstly the pattern of AI variation does not depend on f_{US} value, but there is a trend of increasing reverse current value at the same W_{US} when going to higher frequency USL. Secondly the εI_{US} behavior with the US intensity essentially depends on temperature: the saturation (or non-monotonic relationship at a high bias) and the sharp increase of acoustically driven changes are observed at high and low temperature respectively.

3.2. Leakage current mechanisms

For the purpose of the present consideration, it is important to identify the charge transport mechanisms that control the device characteristics. In order to better understand these mechanisms, we present semi-log current–temperature characteristics at different reverse voltages in Figure 4. As can be clearly seen

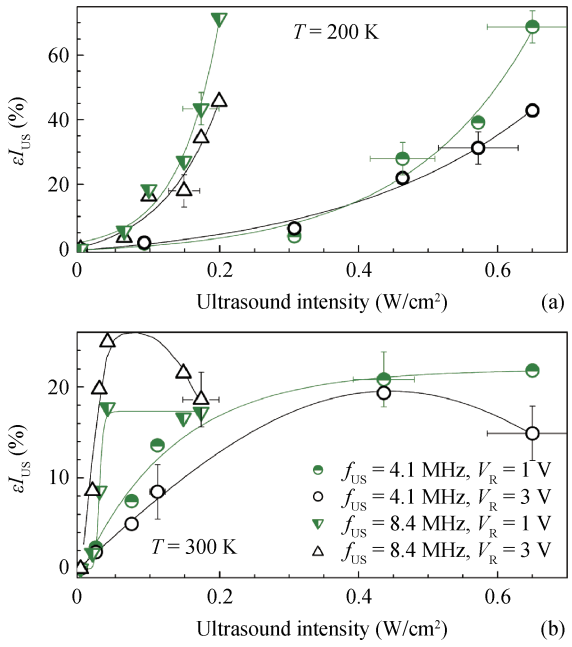

Figure 3. (Color online) Dependences of relative reverse current variation on ultrasonic intensity.

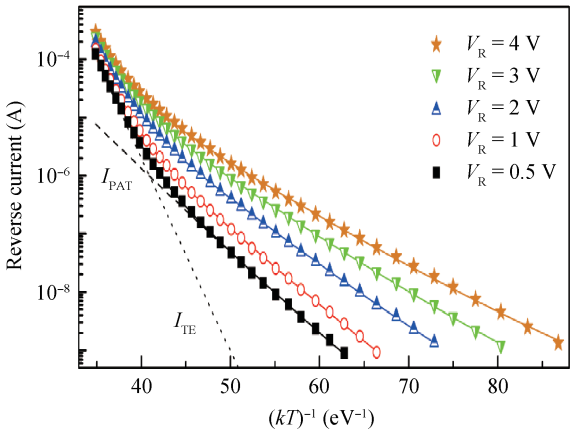

Figure 4. (Color online) Current–temperature characteristics for Mo/n-Si Schottky structures, measured at different reverse bias voltages. The marks are the experimental results, the solid lines are the fitted curves using Equation (11). The dotted and dashed lines represent the TE and the PAT current components respectively for $V_R = 0.5$ V, $W_{us} = 0$.

in the figure, there are two different linear regions there. That is, the current in the structures under study is caused by two different mechanisms and consists of two components I_1 and I_2:

$$I_R(T, V_R) = I_1(T, V_R) + I_2(T, V_R), \quad (1)$$

where T is the sample temperature, V_R is the reverse bias voltage applied to the diode. As mentioned above, the current mechanism diversity can be found in MS structures. On our opinion, one of the components deals with TE current, which is most routine for SDs. Therefore I_1 can be described as follows

$$I_1 = I_0 T^2 \exp(-q\Phi_b/kT)[1 - \exp(-V_R/kT)], \quad (2)$$

where Φ_b is zero bias Schottky barrier height (SBH), I_0 is the constant. It is predicted theoretically[33] and observed experimentally[34,35] that the SBH decreases with temperature increase in a way similar to semiconductor band gap. Therefore we use Varshni equation to calculate the Φ_b temperature dependence:

$$\Phi_b = \Phi_{b0} - 7.021 \times 10^{-4} T^2/(T + 1108), \quad (3)$$

where Φ_{b0} is the SBH at $T = 0$ K.

The SCLC conduction should become important when the density of injected free-charge carriers is much larger than the thermal-generated free-charge-carrier density[27]. So SCLC is more expected at forward bias. The VRHC model yields a low-temperature current with too low activation energies (few meV) at very low electric fields (ohmic regime)[27]. These conditions are far from our case too. As a result, the PAT process is regarded as the second current component. This mechanism is able to explain the dependence of reverse-bias current at wide temperature range and deals with tunneling of electrons from electronic traps, located near the interface layer between electrode and semiconductor, to the conduction band of the semiconductor[23, 29]. The current may be expressed as[23, 36]

$$I_2 = \frac{q^2 E A N_{ss}}{\sqrt{8m^*\epsilon_t}} \sqrt{\frac{\gamma_1 - \gamma}{\gamma_1}} \times \exp\left[-\frac{\sqrt{32m^*\epsilon_t^3}\,(\gamma_1 - \gamma)^2}{3qE\hbar}\left(\gamma_1 + \frac{1}{2}\gamma\right)\right], \quad (4)$$

$$\gamma_1 = (1 + \gamma^2)^{1/2}, \quad (5)$$

$$\gamma = \frac{a\hbar\omega^2\sqrt{2m^*}}{qE\sqrt{\epsilon_t}} \frac{\exp\frac{\hbar\omega}{kT} + 1}{\exp\frac{\hbar\omega}{kT} - 1}, \quad (6)$$

where A is the diode area, N_{ss} is the occupied state density near the interface, m^* is the electron effective mass ($m^* = 1.08m_0$ for Si), ϵ_t is the trap depth to the conduction band, $\hbar\omega$ is the phonon energy, a is the electron–phonon interaction constant, E is the electric field strength on the interface, according to[33]

$$E = \left\{\frac{2qN_d}{\varepsilon_0\varepsilon_s}\left[\Phi_b - \frac{kT}{q}\ln\left(\frac{N_C}{N_d}\right) + V_R\right]\right\}^{1/2}, \quad (7)$$

N_C is the effective density of states in the conduction band, ε_s is the permittivity of the semiconductor (11.7 for Si).

We use Equations (1)–(7) by taking I_0, Φ_{b0}, N_{ss} and ϵ_t as fitting parameters to fit the experimental current–temperature dependences. The value $\hbar\omega = 16$ meV (longitudinal acoustic phonon for Si) and value $a = 6$[29] were chosen to get the best fit of simulated curves to a set of experimental data. The results for I_0 are shown in Figure 5. One can see that I_0 does not remain a constant and decreases with the bias increase. It is evident that the insulating layer has to be taken under consideration. Therefore the applied voltage

$$V_R = V_i + V_s, \quad (8)$$

where V_i and V_s are the voltage drop across the insulating oxide layer and across the depletion region of the semiconductor, respectively. In addition, Equation (1) must be replaced by

$$I_R(T, V_R) = P_t(V_i) \times [I_1(T, V_s) + I_2(T, V_s)], \quad (9)$$

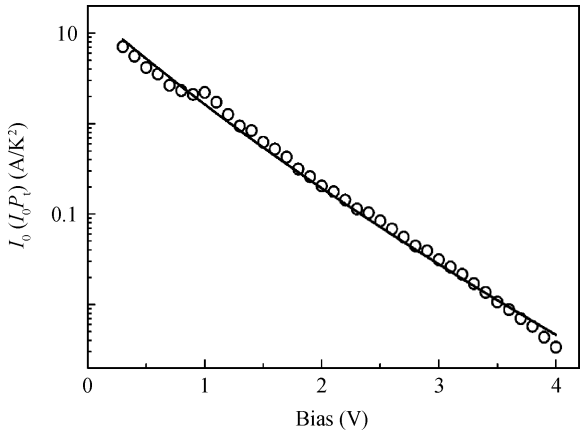

Figure 5. Plot of the temperature-independent factor of TE current component as a function of reverse voltage. Marks are obtained from experimental data, the line is the fitted curve using Equation (10). The calculation was carried out using $V_i = 0.5V_R$.

where P_t is the carrier transfer probability through the insulating layer. Thus Figure 5 does not show I_0 but $P_t I_0$.

In case of the quantum mechanical tunneling through the trapezoid potential barrier, associated with insulating layer, the probability is

$$P_t = \exp\left\{-\frac{4\sqrt{2m_i^* q}}{3\hbar V_i}\left[(U_0 + V_i)^{3/2} - U_0^{3/2}\right]\delta\right\}, \quad (10)$$

where U_0 is zero bias barrier height on the semiconductor/insulator interface, m_i^* is the effective electron mass in the insulator, δ is the insulator thickness. We suppose that $m_i^* = 0.5\, m_0$ (SiO_2) and $V_i = 0.5V_R$ and use Equation (10) to fit data in Figure 5. The result is shown as the solid line. The obtained values of fitting parameters $U_0 = 1$ V and $\delta = 2.8$ nm are realistic and confirm the applicability of used assumptions.

Thereby the generalizing formula of the reverse current is

$$\begin{aligned} I_R &= I_{TE} + I_{PAT} \\ &= P_t I_0 T^2 \exp(-q\Phi_b/kT)[1 - \exp(-V_s/kT)] \\ &\quad + \frac{P_t q^2 E A N_{ss}}{\sqrt{8m^*\epsilon_t}}\left(1 - \frac{\gamma}{\gamma_1}\right)^{1/2} \\ &\quad \times \exp\left\{-\frac{4\sqrt{2m^*}\,\epsilon_t^{3/2}(\gamma_1 - \gamma)^2}{3qE\hbar}\left[\gamma_1 + \frac{1}{2}\gamma\right]\right\}, \quad (11) \end{aligned}$$

where I_{TE} and I_{PAT} are the TE and the PAT current components, respectively and V_R in Equation (7) must be replaced by V_s. We suppose that $V_s = 0.5V_R$ and use Equation (11) to fit the experimental data. The results are shown as the lines in Figure 4. Across the whole bias range the mean square deviation of fitted curves from experimental data is less than 0.7%. The field dependences of extracted parameters are shown in Figure 6, curves 1. The P_t value obtained from Figure 5 data has been used to calculate N_{ss}.

It has been found that the SBH lowering is proportional to E (Figure 6(a))

$$\Phi_{b0} = \Phi_{b00} - \alpha E. \quad (12)$$

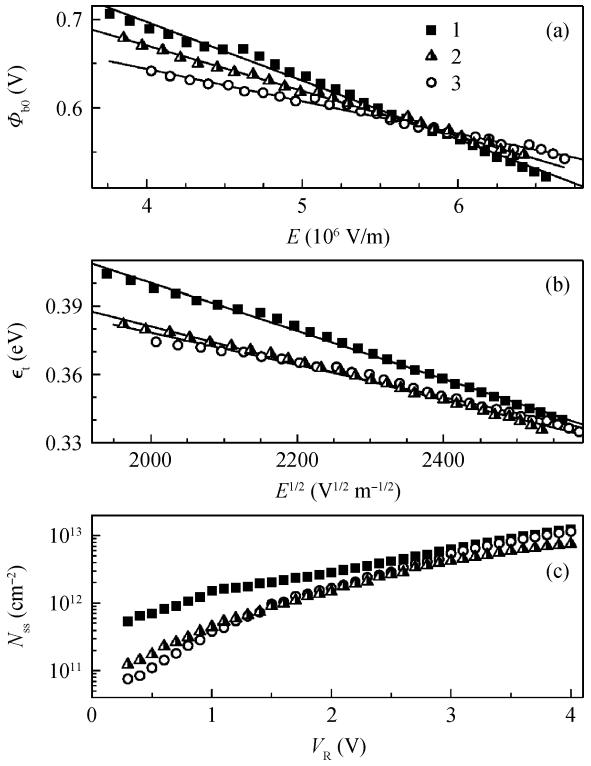

Figure 6. (a) Field dependences of the SBH, (b) the trap depth, and (c) the interface state density for the Mo/n–Si Schottky structures with (2, 3) and without (1) USL. Marks are extracted from experimental data, lines are the linear fitting. W_{US}, W/cm^2: 0 (1), 0.17 (2), 0.65 (3). f_{US}, MHz: 8.4 (2), 4.1 (3).

It is known[30, 33, 37] that similar dependence is observed if the SBH lowering is caused predominantly by interface states. The constant α defines the location of the potential maximum, obtained by superimposing the Schottky field and the surface state field[37].

The obtained ϵ_t (0.35 ÷ 0.40 eV) values are about three times as small as the silicon gap. The similar tendency was previously reported in the PAT current investigation: ϵ_t was equal 0.50 eV for GaAs in Reference [29] and 0.90 eV for GaN in Reference [23]. The trap depth has decreased when going to higher field strength (Figure 6(b))

$$\epsilon_t = \epsilon_{t0} - \beta E^{1/2}, \quad (13)$$

where ϵ_{t0} is the binding energy of the electron on the trap in the zero field. Such mechanism of the field-assisted emission is known as the Poole–Frenkel effect. The value $\epsilon_{t0} = 0.61$ eV is not far from the ionization level for the vacancy type defect in bulk silicon[38, 39]. It is not unlikely that the traps, which assist tunneling, deal with vacancy type defect. The constant β is given by the relation[40, 41]

$$\beta = \sqrt{\frac{Zq^3}{\pi\varepsilon_0\varepsilon_s}}, \quad (14)$$

where Z is the charge multiplicity of the center. In the case of singly charged trap in Si the theoretical value of β_{PF} can be determined using Equation (14) as 2.2×10^{-5} eV(m/V)$^{1/2}$. The experimental values can be different from β_{PF}. On the one

Table 1. Extracted parameters for the Mo/n-Si Schottky structures with and without ultrasonic loading.

W_{US} (W/cm^2)	f_{US} (MHz)	Φ_{b00} (mV)	α (nm)	ϵ_{t0} (meV)	β (10^{-5} eV m$^{1/2}$V$^{-1/2}$)
0	—	960 ± 10	66 ± 7	610 ± 10	10.5 ± 0.3
0.17	8.4	870 ± 10	51 ± 5	540 ± 10	8.1 ± 0.5
0.65	4.1	790 ± 10	36 ± 7	520 ± 10	7.1 ± 0.5

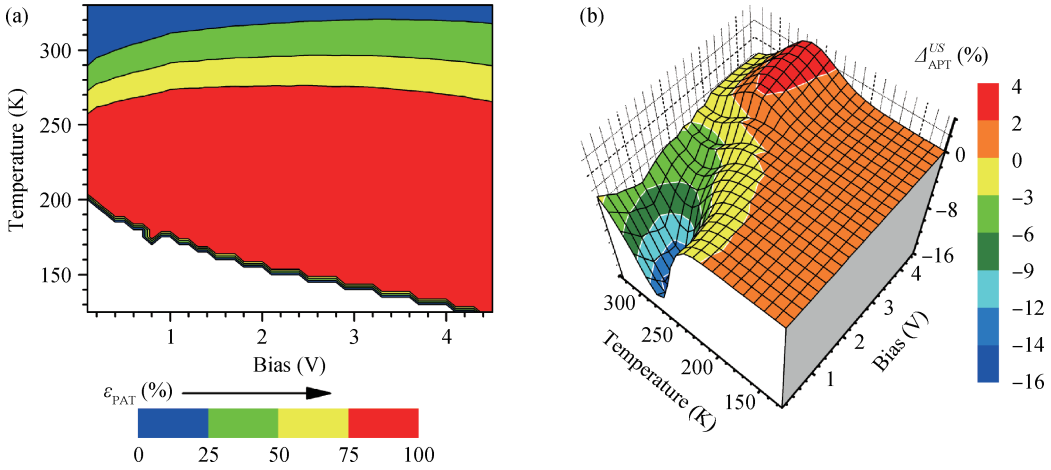

Figure 7. (Color online) (a) Change of the PAT current fractional contribution with the bias and the temperature and (b) its variation under action of ultrasound with $f_{US} = 4.1$ MHz, $W_{US} = 0.65$ W/cm^2.

hand, Equation (14) is valid only for the one-dimensional case and the $\beta < \beta_{PF}$ can be observed experimentally[40, 41]. On the other hand, according to Reference [41], electrons bound on the traps can be located in clusters of positive ions. The cluster creation has fluctuating nature. This phenomena results in an increase of both effective charge multiplicity (up to 10–30[41]) and β value. The magnitude of increasing depends on a cluster size. β value (10.5×10^{-5} eV(m/V)$^{1/2}$) estimated from Figure 6(b) is greater than β_{PF}. In our opinion it is caused by the above mechanism. All obtained parameters results are listed in Table 1 (first data row).

3.3. Effect of ultrasound on charge transport

We use the above described procedure to fit the experimental current–temperature characteristics measured with USL too. The obtained results for two USL mode are summarized on Figure 6 (curves 2 and 3) and in Table 1 (second and third data rows). It has been found that the USL affects the TE current as well as the PAT current. In particular, the trap depth lowering is observed under USL condition, see Figure 6(b). Such effect can be attributed to the change of population of defect oscillator levels[42] or to the displacement of impurity atoms with respect to their surroundings[19]. It is expected[42] that the efficiency of acousto-defect interaction increases with the US frequency growth; this expectation is similar to that which has been observed in our case.

In turn, if an electron requires less energy to escape from the trap then the decreased occupied state density has to be found in the diode with USL. It is a tendency that is observed in our case shown in Figure 6(c). It should be noted, that US influence on traps reduces with electric field growth.

According to Parker *et al.*[37], the α value increases with a penetration distance and density of charged surface states. Therefore a lesser equilibrium number of the surface trapped electrons can be a reason for the observed α decrease under USL condition.

In our opinion AI decrease of β value comes from alteration of a defect cluster size and a following effective charge multiplicity. The probable cause of this phenomenon is the local temperature increase by clusters of point defects under ultrasound action. This effect has been described by Mirzade[43].

It has been found that the SBH decreases under ultrasound action. This result agrees with that which has been obtained from the SD forward (I–V) characteristics[31,44]. It had been shown[44], that the features of SBH variation under USL conditions could be accounted for by the ultrasound absorption by misfit dislocations.

To clarify the voltage–temperature dependence of εI_{US} (Figure 2(b)), the PAT current fractional contribution $\varepsilon_{PAT} = I_{PAT}/(I_{PAT} + I_{TE})$ was taken under consideration.

Figure 7(a) represents the ε_{PAT} voltage–temperature dependence for the sample without USL and Figure 7(b) shows the ε_{PAT} variation under ultrasound action ($\Delta^{US}_{PAT} = \varepsilon^{US}_{PAT} - \varepsilon_{PAT}$, where ε^{US}_{PAT} corresponds to the diode with USL).

As one can recognize, the PAT reverse current component is prevalent at low temperature, whereas the TE current contribution becomes important at $T > 260$ K. In addition, it has to be taken into consideration that (i) the decrements of ϵ_{t0} and β (as well as Φ_{b00} and α) have opposite influence on reverse current value; (ii) the SBH has stronger dependence on electric field than the trap depth (the Φ_{b0} and ϵ_t variation with E is 25% and 15% respectively—see Figure (6), but the PAT current is implicitly dependent on E—see Equation (4).

We calculated the current ratio $\frac{I(\theta-\Delta_\theta)}{I(\theta)}$, where $I(\theta)$ and $I(\theta - \Delta_\theta)$ are the current before and after parameter θ reduc-

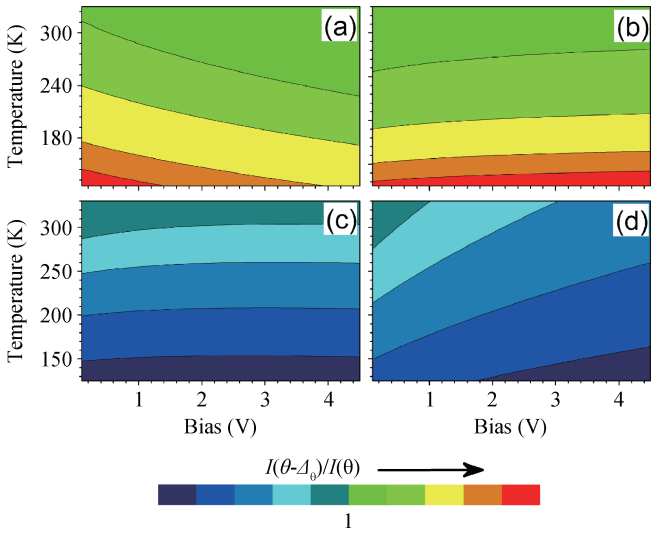

Figure 8. (Color online) Qualitative pattern of TE (a, c) and PAT (b, d) current variation with decrease of trap depth (a), SBH at zero temperature (b), Poole–Frenkel factor (c) and factor of interface states influence on SBH (d). Equations (2), (4), (12) and (13) were used to calculate the presented data. See details in the text.

tion, θ is one of $\{\epsilon_{t0}, \beta, \Phi_{b00}, \alpha\}$. The results are presented on Figure 8. Thereby the reverse current increase is determined by the AI ϵ_{t0} decrease in the temperature range 130–250 K. This effect is slightly compensated by the β and N_{ss} decrease. If the TE reverse current is important, then the effect of SBH variation comes to the foreground. But the Φ_{b00} decrease effect is considerably masked by the α decrease. In particular, this masking leads to PAT contribution increasing at middle temperatures (250–300 K) and high bias ($V_R > 3.5$ V) (Figure 7(b)). As it is assumed above, the change of Φ_{b00} and α is due to ultrasound absorption by misfit dislocations and to AI reduction of surface trapped electrons respectively. These phenomena depend on ultrasound intensity in different way. As a result the non-monotonic dependence of εI_{US} on W_{US} is observed at high bias (Figure 3(b)).

4. Conclusion

The experimental investigation of ultrasound influence on the reverse leakage current of Mo/n–n^+-Si Schottky barrier structure has been carried out in the temperature range from 130 to 330 K. The investigation has revealed the acoustically induced reversible increase of reverse current. The efficiency of ultrasound influence decreases with the bias and the temperature rising and increases with the acoustic waves frequency growth. The analysis has shown that the thermionic emission and the phonon-assisted tunneling make a major contribution to the leakage current and both mechanisms are affected by ultrasound. It has been found that the ultrasonic loading leads to the decrease of barrier height, trap depth, occupied interface state density, Poole–Frenkel factor. Thus, ultrasound can be an effective tool for controlling metal–semiconductor structure characteristics.

References

[1] Savkina R K, Smirnov A B, Sizov F. The effect of high-frequency sonication on charge carrier transport in LPE and MBE HgCdTe layers. Semicond Sci Technol, 2007, 22(2): 97
[2] Kulakova L, Gorelov V, Lutetskiy A, et al. The rotation of the polarization plane of quantum-well heterolasers emission under the ultrasonic strain. Solid State Commun, 2012, 152(17): 1690
[3] Ostrovskii I, Korotchenkov O, Olikh O, et al. Acoustically driven optical phenomena in bulk and low-dimensional semiconductors. J Opt A, 2001, 3(4): S82
[4] Buyukkose S, Vratzov B, van der Veen J, et al. Ultrahigh-frequency surface acoustic wave generation for acoustic charge transport in silicon. Appl Phys Lett, 2013, 102(1): 013112
[5] He J H, Gao J, Guo H Z. Correlated electron transport assisted by surface acoustic waves in micron-separated quasi-one-dimensional channels. Appl Phys Lett, 2010, 97(12): 122107
[6] Ostapenko S S, L Jastrzebski, Sopori B. Change of minority carrier diffusion length in polycrystalline silicon by ultrasound treatment. Semicond Sci Technol, 1995, 10(11): 1494
[7] Ostapenko S. Defect passivation using ultrasound treatment: fundamentals and application. Appl Phys A: Mater Sci Process, 1999, 69(2): 225
[8] Sukach A, Teterkin V. Ultrasonic treatment-induced modification of the electrical properties of InAs p–n junctions. Tech Phys Lett, 2009, 35(6): 514
[9] Olikh O. Features of dynamic acoustically induced modification of photovoltaic parameters of silicon solar cells. Semiconductors, 2011, 45(6): 798
[10] Davletova A, Karazhanov S Z. A study of electrical properties of dislocation engineered Si processed by ultrasound. J Phys Chem Solids, 2009, 70(6): 989
[11] Davletova A, Karazhanov S Z. Open-circuit voltage decay transient in dislocation-engineered Si p–n junction. J Phys D: Appl Phys, 2008, 41(16): 165107
[12] Melnik V, Olikh Y, Popov V, et al. Characteristics of silicon p–n junction formed by ion implantation with *in situ* ultrasound treatment. Mater Sci Eng B, 2005, 124/125: 327
[13] Olikh O. Effect of ultrasonic loading on current in Mo/n–n+-Si with Schottky barriers. Semiconductors, 2013, 47(7): 987
[14] Olikh O. Reversible influence of ultrasound on γ-irradiated Mo/n-Si Schottky barrier structure. Ultrasonics, 2015, 56: 545
[15] Zaveryukhina N, Zaveryukhina E, Vlasov S, et al. Acoustostimulated changes in the density of surface states and their energy spectrum in p-type silicon single crystals. Tech Phys Lett, 2008, 34(3): 241
[16] Mirsagatov S A, Sapaeva I B, Nazarov Z. Ultrasonic annealing of surface states in the heterojunction of a p-Si/n-CdS/n^+-CdS injection photodiode. Inorg Mater, 2015, 51(1): 1
[17] Wosinski T, Makosa A, Witczak Z. Transformation of native defects in bulk GaAs under ultrasonic vibration. Semicond Sci Technol, 1994, 9(11): 2047
[18] Buyanova I A, Ostapenko S S, Sheinkman M K, et al. Ultrasound regeneration of EL2 centres in GaAs. Semicond Sci Technol, 1994, 9(2): 158
[19] Korotchenkov O, Grimmliss H. Long-wavelength acoustic-mode-enhanced electron emission from Se and Te donors in silicon. Phys Rev B, 1995, 52(20): 14598
[20] Ostapenko S S, Bell R E. Ultrasound stimulated dissociation of Fe–B pairs in silicon. J Appl Phys, 1995, 77(10): 5458
[21] Sathaiya D M, Karmalkar S. Thermionic trap-assisted tunneling model and its application to leakage current in nitrided oxides and AlGaN/GaN high electron mobility transistors. J Appl Phys,

2006, 99(9): 093701
[22] Shan Q, Meyaard D S, Dai Q, et al. Transport-mechanism analysis of the reverse leakage current in GaInN light-emitting diodes. Appl Phys Lett, 2011, 99(25): 253506
[23] Pipinys P, Lapeika V. Temperature dependence of reverse-bias leakage current in GaN Schottky diodes as a consequence of phonon-assisted tunneling. J Appl Phys, 2006, 99(9): 093709
[24] Liang Huaguo, Xu Hui, Huang Zhengfeng, et al. Low-leakage and NBTI-mitigated N-type domino logic. Journal of Semiconductors, 2014, 35(1): 015009
[25] Bi Xiuwen, Liang Hailian, Gu Xiaofeng, et al. Design of novel DDSCR with embedded PNP structure for ESD protection. Journal of Semiconductors, 2015, 36(12): 124007
[26] Abu-Samaha F S, Darwish A A A, Mansour A N. Temperature dependent of the current–voltage (IV) characteristics of $TaSi_2$/n-Si structure. Mater Sci Semicond Process, 2013, 16(6): 1988
[27] Jafar M M A G. High-bias current–voltage–temperature characteristics of undoped RF magnetron sputter deposited boron carbide (B_5C)/p-type crystalline silicon heterojunctions. Semicond Sci Technol, 2003, 18(1): 7
[28] Lee C H, Lim K S. Carrier transport through boron-doped amorphous diamond-like carbon p layer of amorphous silicon based p–i–n solar cells. Appl Phys Lett, 1999, 75(4): 569
[29] Pipinys P, Pipiniene A, Rimeika A. Phonon-assisted tunneling in reverse biased Schottky diodes. J Appl Phys, 1999, 86(12): 6875
[30] Tung R T. Recent advances in Schottky barrier concept. Mater Sci Eng, R, 2001, 35(1–3): 1
[31] Olikh O Y, Voytenko K V, Burbelo R M. Ultrasound influence on I–V–T characteristics of silicon Schottky barrier structure. J Appl Phys, 2015, 117(4): 044505
[32] Wang K, Ye M. Parameter determination of Schottky-barrier diode model using differential evolution. Solid-State Electron, 2009, 53(2): 234
[33] Rhoderick E H, Williams R H. Metal semiconductor contacts. 2nd ed. Oxford: Clarendon Press, 1988
[34] Aboelfotoh M. Electrical characteristics of W–Si(100) Schottky barrier junctions. J Appl Phys, 1989, 66(1): 262
[35] Zhua S, Meirhaeghea R L V, Detaverniera C, et al. A BEEM study of the temperature dependence of the barrier height distribution in PtSi/n-Si Schottky diodes. Solid State Commun, 1999, 112(11): 611
[36] Kiveris A, Kudzmauskas S, P P. Release of electrons from traps by an electric field with phonon participation. Phys Stat Sol (a), 1976, 37(1): 321
[37] Parker G, McGill T, Mead C, et al. Electric field dependence of GaAs Schottky barriers. Solid-State Electron, 1968, 11(2): 201
[38] Seebauer E G, Kratzer M C. Charged point defects in semiconductors. Mater Sci Eng R, 2006, 55(3–6): 57
[39] Lukjanitsa V V. Energy levels of vacancies and interstitial atoms in the band gap of silicon. Semiconductors, 2003, 37(4): 404
[40] Mitrofanov O, Manfra M. Poole-Frenkel electron emission from the traps in AlGaN/GaN 13 transistors. J Appl Phys, 2004, 95(11): 6414
[41] Zhdanova N G, Kagan M S, Landsberg E G, et al. Ionization of shallow impurities by the electric field in a random coulomb potential. JETP Lett, 1995, 62(2): 119
[42] Pavlovich V N. Enhanced diffusion of impurities and defects in crystals in conditions of ultrasonic and radiative excitation of the crystal lattice. Phys Stat Sol (b), 1993, 180(1): 97
[43] Mirzade F. Elastic wave propagation in a solid layer with laser-induced point defects. J Appl Phys, 2011, 110(6): 064906
[44] Olikh O, Voytenko K. On the mechanism of ultrasonic loading effect in silicon-based Schottky diodes. Ultrasonics, 2016, 66(1): 1